Three-dimensional image formation in fiber-optical second-harmonic-generation microscopy

Min Gu and Ling Fu

Centre for Micro-Photonics, Faculty of Engineering and Industrial Sciences, Swinburne University of Technology, P. O. Box 218, Hawthorn, Victoria 3122, Australia
mgu@swin.edu.au

Abstract: Three-dimensional (3-D) image formation in fiber-optical second-harmonic-generation microscopy is revealed to be purely coherent and therefore can be described by a 3-D coherent transfer function (CTF) that exhibits the same spatial frequency passband as that of fiber-optical reflection-mode non-fluorescence microscopy. When the numerical aperture of the fiber is much larger than the angle of convergence of the illumination on the fiber aperture, the performance of fiber-optical second-harmonic-generation microscopy behaves as confocal second-harmonic-generation microscopy. The dependence of axial resolution on fiber coupling parameters shows an improvement of approximately 7%, compared with that in fiber-optical two-photon fluorescence microscopy.

OCIS codes: (180.6900) Three-dimensional microscopy; (110.2990) Image formation theory; (110.2350) Fiber optics imaging

References and links

1. J. N. Gannaway and C. J. R. Sheppard, "Second-harmonic imaging in the optical scanning microscope," Opt. Quantum Electron. **10,** 435 (1978).
2. Y. Guo, P. P. Ho, H. Savage, D. Harris, P. Sacks, S. Schantz, F. Liu, N. Zhadin, and R. R. Alfano, "Optical harmonic generation from animal tissue by the use of picosecond and femtosecond laser pulses," Opt. Lett. **22**, 1323 (1997).
3. P. J. Campagnola and L. M. Loew, "Second harmonic imaging microscopy for visualizing biomolecular arrays in cells, tissues and organisms," Nat. Biotech. **21**, 1356 (2003).
4. W. R. Zipfel, R. M. Williams, and W. W. Webb, "Nonlinear magic: multiphoton microscopy in the biosciences," Nat. Biotech. **21**, 1369 (2003).
5. R. Gauderon, P. B. Lukins, and C. J. R. Sheppard, "Three-dimensional second-harmonic generation imaging with femtosecond laser pulses," Opt. Lett. **23,** 1209 (1998).
6. W. Denk, J. H. Strickler, and W. W. Webb, "Two photon laser scanning fluorescence microscopy," Science **248**, 73 (1990).
7. D. Bird and M. Gu, "Compact two-photon fluorescence microscope based on a single-mode fiber coupler," Opt. Lett. **27**, 1031 (2002).
8. D. Bird and M. Gu, "Two-photon fluorescence endoscopy with a micro-optic scanning head," Opt. Lett. **28**, 1552 (2003).
9. D. Bird and M. Gu, "Fiber-optic two-photon scanning fluorescence microscopy," J. Micros. **208,** 35 (2002).
10. L. Fu, X. Gan, and M. Gu, "Use of single-mode fiber coupler for second-harmonic-generation microscopy," Opt. Lett. **30**, 385 (2005).
11. L. Fu, X. Gan, and M. Gu, "Nonlinear optical microscopy based on double-clad photonic crystal fibers," Opt. Expess **13**, 5528 (2005).
12. M. Gu, *Principles of Three-Dimensional Imaging in Confocal Microscopes* (World Scientific, Singapore, 1996).
13. C. J. R. Sheppard and M. Gu, "The significance of 3D transfer functions in confocal scanning microscopy," J. Micros. **165,** 377 (1992).
14. M. Gu and D. Bird, "Three-dimensional optical-transfer-function analysis of fiber-optical two-photon fluorescence microscopy," J. Opt. Soc. Am. A **20,** 941 (2003).
15. M. Gu, C. J. R. Sheppard, and X. Gan, "Image formation in a fiber-optical confocal scanning microscope" J. Opt. Soc. Am. A **8**, 1755 (1991).
16. S. Kimura and T. Wilson, "Confocal scanning optical microscope using single-mode fiber for signal detection," Appl. Opt. **30**, 2143 (1991).

#9309 - $15.00 USD Received 28 October 2005; revised 23 January 2006; accepted 23 January 2006

17. M. Gu, X. Gan, and C. J. R. Sheppard, "Three-dimensional coherent transfer functions in fiber-optical confocal scanning microscopes," J. Opt. Soc. Am. A **8**, 1019 (1991).
18. S. Yazdanfar, L. H. Laiho, and P. T. C. So, "Interferometric second harmonic generation microscopy," Opt. Express **12**, 2739 (2004).
19. M. Gu and C. J. R. Sheppard, "Comparison of three-dimensional imaging properties between two-photon and single-photon fluorescence microscopy," J. Micros. **177,** 128 (1995).

1. Introduction

Second-harmonic-generation (SHG) microscopy was proposed by Gannaway and Sheppard in 1970s [1] and has been recently extensively explored for biological studies [2-5]. Together with two-photon (2-p) excited fluorescence microscopy [6], SHG microscopy provides the cellular-level functionality and morphology information of a sample, an inherent sectioning ability for three-dimensional (3-D) imaging, and relatively deep optical penetration within biological tissue [2-6]. In order to apply these new nonlinear optical imaging techniques into *in vivo* applications, fiber-optical components such as a fiber coupler have been adopted for miniaturization [7-11]. Physically, 2-p excited fluorescence and SHG microscopy corresponds to incoherent and coherent imaging processes which can be understood by an optical transfer function and a coherent transfer function (CTF) [12, 13], respectively. Therefore, a 3-D optical transfer function has been derived to describe the imaging performance in fiber-optical 2-p fluorescence microscopy [14]. However, such a description is not applicable to fiber-optical SHG microscopy.

In the case of a non-fluorescent linear sample, fiber-optical scanning microscopy behaves fully coherently even for finite values of fiber spot size [15, 16] and therefore can be described by a 3-D CTF that can be expressed by an analytical expression [17]. The aim of this paper is to understand 3-D image formation in fiber-optical SHG microscopy using the concept of the 3-D CTF and to reveal the dependence of axial resolution on fiber coupling parameters.

2. Three-dimensional coherent transfer function in fiber-optical SHG microscope

In order to investigate the effect of optical fibers on illumination and collection separately, let us consider the schematic diagram of a fiber-optical SHG microscope as shown in Fig. 1. Two optical single-mode fibers F_1 and F_2 are used to deliver illumination at wavelength $2\lambda_0$ and collect SHG signal at wavelength λ_0, respectively. When the illumination optical fiber F_1 and the collection optical fiber F_2 are identical, the performance of the system is equivalent to that using a fiber coupler [10]. As SHG is a coherent process, the analysis of image formation in fiber-optical SHG microscopy is similar to that in fiber-optical non-fluorescence microscopy described elsewhere [17]. Considering that the electrical field of the SHG emission from a sample is proportional to the square of the field of the illumination field on the sample, the image intensity from a scan point $\boldsymbol{r}_s = (x_s, y_s, z_s)$ in the fiber-optical SHG microscope can be expressed, if the optical axis is assumed along the *z* direction, as

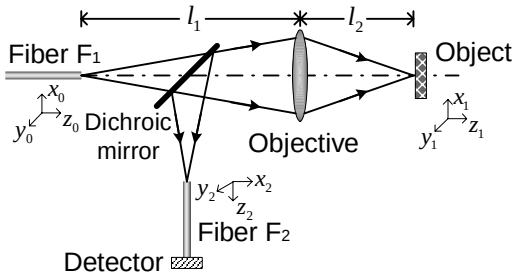

Fig. 1. Schematic diagram of the fiber-optical SHG scanning microscope.

#9309 - $15.00 USD Received 28 October 2005; revised 23 January 2006; accepted 23 January 2006

$$I(\boldsymbol{r}_s) = \Big| \int_{-\infty}^{\infty} U_2^*(x_2, y_2)\delta(z_2)\left[\int_{-\infty}^{\infty} U_1(x_0, y_0)\delta(z_0)\exp[ik(z_0 - z_1)]h_1(\boldsymbol{r}_0 + \boldsymbol{M}_1\boldsymbol{r}_1)d\boldsymbol{r}_0\right]^2 \varepsilon(\boldsymbol{r}_s - \boldsymbol{r}_1)\exp[ik(\pm z_1 - z_2)]h_2(\boldsymbol{r}_1 + \boldsymbol{M}_2\boldsymbol{r}_2)d\boldsymbol{r}_2 d\boldsymbol{r}_1\Big|^2, \quad (1)$$

where the letters $\boldsymbol{r}_i$ (i=0,1,2) represent vectors with components x_i, y_i, z_i. The functions $U_1(x, y)$ and $U_2(x, y)$ are the amplitude mode profile on the output end of fiber F_1 and on the input end of fiber F_2, respectively. * denotes the conjugate operation and the parameters $\boldsymbol{M}_1$ and $\boldsymbol{M}_2$ are diagonal matrices of the magnification factors of the illumination and collection lenses, respectively. The term in the first square brackets results from the quadratic dependence of SHG. $h_1(\boldsymbol{r})$ and $h_2(\boldsymbol{r})$ are the 3-D amplitude point spread functions (PSFs) for the objective in illumination and collection paths, respectively [17]. $\varepsilon(\boldsymbol{r})$ is the object function representing the SHG strength of the object. Using the 3-D convolution relation, one can simplify Eq. (1) as

$$I(\boldsymbol{r}_s) = \left|h_{eff}(\boldsymbol{r}_s) \otimes_3 \varepsilon(\boldsymbol{r}_s)\right|^2, \quad (2)$$

where $\otimes_3$ denotes the 3-D convolution operation. h_{eff} is the 3-D effective PSF for fiber-optical SHG microscopy and given by

$$h_{eff}(\boldsymbol{r}) = \left[U_1(\boldsymbol{M}_1 x, \boldsymbol{M}_1 y) \otimes_2 h_1(\boldsymbol{M}_1\boldsymbol{r})\right]^2 \left[U_2^*(\boldsymbol{M}_1 x, \boldsymbol{M}_1 y) \otimes_2 h_2(\boldsymbol{r})\right]. \quad (3)$$

Here $\otimes_2$ denotes the 2-D convolution operation.

It is necessary to point out that Eqs. (1) and (2) represent a superposition of the light amplitude from a sample and therefore implies that like fiber-optical non-fluorescence microscopy [15-17] fiber-optical SHG microscopy is purely coherent. This feature is of particular importance when one performs SHG interferometric microscopy/tomography [18]. Therefore, fiber-optical SHG microscopy can be analyzed in terms of the 3-D CTF that is given by the 3-D Fourier transform of the effective PSF [12, 17]. The 3-D CTF, $c(\boldsymbol{m})$, for fiber-optical SHG microscope can thus be described by

$$c(\boldsymbol{m}) = c_1(\boldsymbol{m}) \otimes_3 c_2(\boldsymbol{m}), \quad (4)$$

where

$$c_1(\boldsymbol{m}) = F_3\left\{\left[U_1(\boldsymbol{M}_1 x, \boldsymbol{M}_1 y) \otimes_2 h_1(\boldsymbol{M}_1\boldsymbol{r})\right]^2\right\}, \quad (5)$$

and

$$c_2(\boldsymbol{m}) = F_3\left\{U_2^*(\boldsymbol{M}_1 x, \boldsymbol{M}_1 y) \otimes_2 h_2(\boldsymbol{r})\right\}. \quad (6)$$

Here F_3 is the 3-D Fourier transform with respect to $\boldsymbol{r}_s$ and $\boldsymbol{m}$ represents the spatial frequency vector with two transverse components m and n, and one axial component s. For a system using a circular lens, $c_1(\boldsymbol{m})$ is the 3-D CTF for a fiber-optical reflection-mode non-fluorescence microscope with wavelength $2\lambda_0$ [17] and can be analytically expressed as:

$$c_1(l, s) = \exp(-2A_1 s)\begin{cases} 1 & , \quad l^2/2 \le s \le 1/2 - l(1-l), \\ (2/\pi)\sin^{-1}\left\{(1-2s)/[2l(2s-l^2)^{1/2}]\right\} & , \quad 1/2 - l(1-l) \le s \le 1/2, \\ 0 & , \quad \textit{otherwise.} \end{cases} \quad (7)$$

Similarly, Eq. (6) represents the 3-D CTF for a single circular lens with wavelength λ_0 and weighted by the Fourier transform of the fiber mode profile $U_2^*(x, y)$, given by

#9309 - $15.00 USD Received 28 October 2005; revised 23 January 2006; accepted 23 January 2006

$$c_2(l,s) = \exp(-A_2 l^2/2)\delta(s - l^2/2)\,. \tag{8}$$

In Eqs. (7) and (8), $A_j = [2\pi a a_j/(\lambda_j d_j)]^2$ (j = 1, 2) is the normalized fiber spot size for illumination and collection fibers. d_j is the distance between the fiber ends and the objective. The variables l ($l=\sqrt{m^2+n^2}$) and s denote the radial and axial spatial frequencies normalized by $\sin\alpha/\lambda_0$ and $4\sin^2(\alpha/2)/\lambda_0$, respectively, where $\sin\alpha$ is the numerical aperture of the objective of radius a. Here we have assumed that both illumination and collection fibers are single-mode fibers of mode spot radii a_1 and a_2. It has been shown that A_j is proportional to the square of the ratio of the numerical aperture of the objective in the illumination and collection paths to the numerical aperture of the fibers F_1 and F_2 [12].

According to Eq. (4), the 3-D CTF can be numerically evaluated, if the delta function in Eq. (8) is taken into account, by

$$c(l,s) = \iint_{\sigma} \exp\left[\frac{-A_2(m^2+n^2)}{2}\right] c_1\left(\sqrt{(m-l)^2+n^2}, s - \frac{m^2+n^2}{2}\right) dm\,dn\,, \tag{9}$$

where σ represents the area overlapped by $m^2+n^2=1$ and $(m-l)^2+n^2=1$. Finally, 3-D CTF for fiber-optical SHG microscopy can be explicitly written as

$$c(l,s) = \int_0^{\sqrt{1-(l/2)^2}} \left[\int_{l-\sqrt{1-n^2}}^{\sqrt{1-n^2}} \exp\left[\frac{-A_2(m^2+n^2)}{2}\right] c_1\left(\sqrt{(m-l)^2+n^2}, s - \frac{m^2+n^2}{2}\right) dm\right] dn\,. \tag{10}$$

It should be pointed out that 3-D CTF for fiber-optical SHG microscopy has a spatial frequency passband of $l^2/4 < (s+s0) < 1$ with axial and transverse cutoffs 1 and 2, respectively. Here $s0 = 1/[2\sin^2(\alpha/2)]$ is a constant axial spatial-frequency shift resulting from the reflection imaging geometry [12]. This feature is the same as fiber-optical reflection-mode non-fluorescence microscopy [17].

3. Results and discussion

When $A_j \to 0$, which corresponds to the case when the numerical aperture of the fiber is

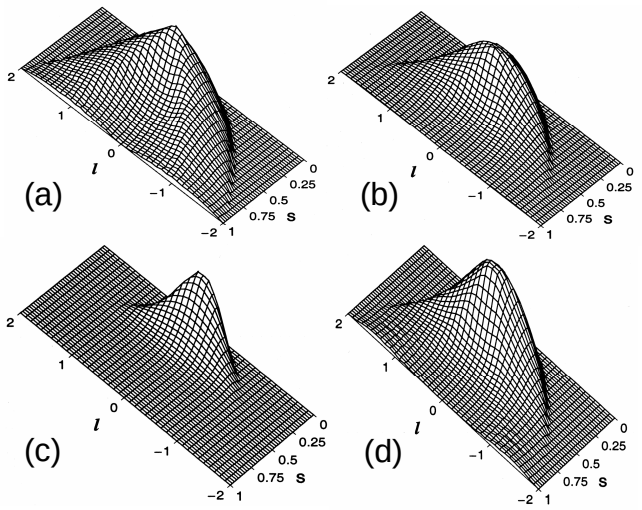

Fig. 2. 3-D CTF for fiber-optical SHG microscopy. (a) A_1 = 0, A_2=4A_1. (b) A_1 = 1, A_2=4A_1.

#9309 - $15.00 USD Received 28 October 2005; revised 23 January 2006; accepted 23 January 2006

much larger than that of the objective in illumination and collection paths, the 3-D CTF describes confocal SHG microscopy of a point source and a point detector. If either A_1 or A_2 becomes infinity, $c(l,s)$ becomes Eq. (8) or Eq. (7). No image is formed because $c(l,s)$ is zero. For a SHG microscope based on a fiber coupler [10], we have $4A_1 = A_2$ and the corresponding 3-D CTFs for A_1 = 0, 1, 5 are shown in Figs. 2(a)-(c). Figure 2(a) represents the 3-D CTF for confocal SHG microscopy with a point source and a point detection. For a finite value of A_1, the strength of the 3-D CTF is reduced in particular along the axial direction, as shown in Figs. 2(b) and (c). Figure 2(d) also denotes the 3-D CTF when a point source is used (A_1 = 0) and a fiber is used for collection. In this case, the collection function of the objective becomes weak. Ultimately, when $A_2 \to \infty$, $c_2(l,s)$ approaches a delta function at l = 0 and thus the 3-D CTF for SHG microscopy is given by Eq. (7).

It is important to investigate the axial cross section, $c(l=0,s)$ of the 3-D CTF further as it gives the axial imaging performance. The solid curves in Fig. 3 represent the normalized axial cross section of the 3-D CTF for SHG microscopy using a fiber coupler ($4A_1 = A_2$), while the dashed line depicts the condition for $A_1 = 0$ and $A_2 \to \infty$. For $4A_1 = A_2 = 0$, the CTF increases linearly up to s = 1/3, which is contributed by the constant region in Eq. (7). After the maximum value at s = 1/3, the CTF decreases and finally cuts off at s = 1. When $4A_1 = A_2$ and $A_1 \neq 0$, the strength of the CTF for s <1/3 is enhanced while that for s >1/3 is reduced. When eventually $4A_1 = A_2 \to \infty$, the CTF approaches a delta function at s = 0, which means that there is no axial imaging ability.

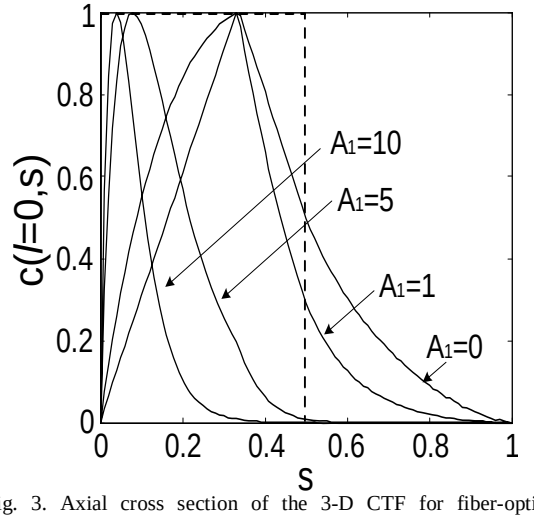

Fig. 3. Axial cross section of the 3-D CTF for fiber-optical SHG microscopy using a fiber coupler (A_2=4A_1) for different values of the normalized optical spot size parameter A_1. The dashed curve represents the case for A_1 = 0 and $A_2 \to \infty$.

To characterize axial resolution, one usually considers imaging of a perfect SHG reflector scanning through the focus of the objective. This axial response is a measure of axial resolution or the optical sectioning property [10, 11] and can be calculated using the modulus squared of the Fourier transform of the axial cross section of the 3-D CTF at l = 0 [12, 17]. After mathematical manipulations, such an axial response can be expressed as

$$I(u) = \left| \int_0^1 \left\{ \int \frac{\exp\{-l^2[(A_1 - iu/2) + (A_2 - iu)/2]\}}{A_1 - iu/2} \left\{1 - \exp[-\rho_0^2 (A_1 - iu/2)]\right\} d\theta \right\} l dl \right|^2, \quad (11)$$

#9309 - $15.00 USD Received 28 October 2005; revised 23 January 2006; accepted 23 January 2006

where $\rho_0 = -l\cos\theta + \sqrt{1-l^2\sin^2\theta}$ and $u = (8\pi/\lambda_0)z\sin^2(\alpha/2)$.

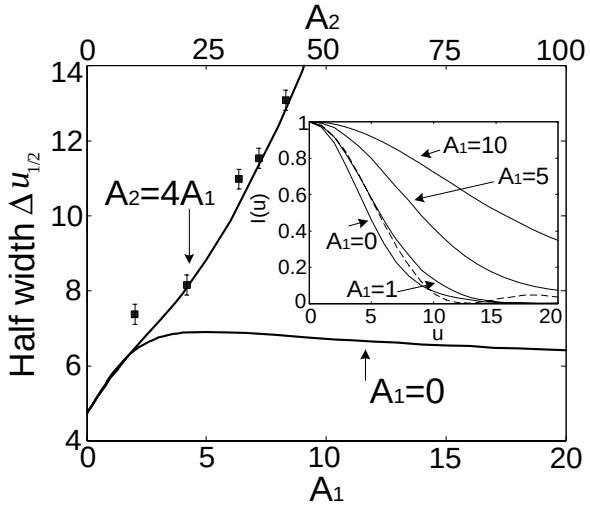

Fig. 4. Half width at half maximum of the axial response, $\Delta u_{1/2}$, as a function of the normalized fiber spot size parameter when $A_2=4A_1$ (bottom axis) and when $A_1 = 0$ (up axis). The squares are experimental results for A_1 =2.0, 4.2, 6.4, 7.3, 8.4, respectively. Inset: Normalized axial response of a perfect SHG reflector in fiber-optical SHG microscopy using a fiber coupler ($A_2=4A_1$) for different values of the normalized optical spot size parameter A_1. The dashed curve represents the case for $A_1 = 0$ and $A_2 \to \infty$.

The normalized SHG axial response and the half width at half maximum (HWHM, $\Delta u_{1/2}$) as a function of the normalized fiber spot size parameters A_j are shown in Fig. 4. It shows that the SHG axial resolution approaches 5.57 for $A_1 = 0$ and $A_2 \to \infty$. In this case, Eq. (11) reduces to $I(u) = [\sin(u/4)/(u/4)]^2$ and is depicted as a dashed curve in the inset of Fig. 4, which confirms that SHG microscopy exhibits an inherent optical section property without necessarily using finite-sized detection. This feature also implies that SHG microscopy has an improvement of axial resolution by 35% compared with 2-p fluorescence microscopy without any pinhole [19].

In the case of SHG microscopy using a fiber coupler [10], the HWHM is approximately 4.72 for $4A_1 = A_2 = 0$. The HWHM as a function of A_1 exhibits a linear dependence when $A_1 > 5$. Under the experimental conditions [10] of A_1 = 2.0, 4.2, 6.4, 7.3, 8.4, the measured values of $\Delta u_{1/2}$ are shown as square spots in Fig. 4. $\Delta u_{1/2}$ is derived from the axial response of the fiber-optic SHG microscope to a thin layer of AF-50 dye. Parameter A_1 is varied by using various values of numerical apertures of the objective to couple the SHG signal into the single-mode fiber coupler. It is shown that experimental results further confirm the dependence of the axial resolution on the normalized fiber spot size parameters. The deviations between the theory and the experimental data might be due to the presence of spherical aberration and the finite thickness of the SHG layer. Compared with the HWHM in fiber-optical 2-p fluorescence microscopy [14], the axial resolution in fiber-optical SHG microscopy is increased approximately by 7%.

#9309 - $15.00 USD Received 28 October 2005; revised 23 January 2006; accepted 23 January 2006

4. Conclusions

In conclusion, the 3-D CTF has been reported to analyze the three-dimensional image formation in fiber-optical SHG microscopy. Its spatial frequency passband is identical to that for fiber-optical reflection-model non-fluorescence microscopy though the strength of the 3-D CTF is reduced due to the finite-sized fiber aperture. For a system based on a fiber coupler and a given illumination wavelength, the axial resolution in SHG microscopy is increased approximately by 7%, compared with 2-p fluorescence microscopy.

Acknowledgments

The authors thank the Australian Research Council for its support.

#9309 - $15.00 USD Received 28 October 2005; revised 23 January 2006; accepted 23 January 2006